Scientific Journals
of the Maritime University of Szczecin

Zeszyty Naukowe
Akademii Morskiej w Szczecinie

2020, 62 (134), 108–115
ISSN 1733-8670 (Printed)
ISSN 2392-0378 (Online)
DOI: 10.17402/425

Received: 09.12.2019
Accepted: 08.04.2020
Published: 29.06.2020

Calculating the second-order hydrodynamic force on fixed and floating tandem cylinders

Mohammad Motallebi[1], Hamidreza Ghafari[2], Hassan Ghassemi[2]✉, Mehdi Shokouhian[3]

Amirkabir University of Technology, Tehran, Iran
[1] Department of Civil and Environmental Engineering, e-mail: m_motallebi@aut.ac.ir
[2] Department of Maritime Engineering, e-mail: hamidrezaghafari@aut.ac.ir, gasemi@aut.ac.ir
[3] Morgan State University, Department of Civil Engineering, Baltimore, USA
✉ corresponding author

Key words: fixed cylinder, floating cylinder, second order hydrodynamic force, diffracted wave, potential theory

Abstract

In this paper, the second-order hydrodynamic force on fixed and floating tandem cylinders has been calculated and different parameters have been taken into consideration. An incident wave is diffracted by the fixed cylinder, and as a result low-frequency waves radiate toward the floating cylinder and cause low-frequency second-order hydrodynamic forces to act on the surface of the floating cylinder. The interactions between the fixed and floating cylinders have been investigated by changing the distance between them, as well as the draft and radius of the floating cylinder. By employing perturbation series analysis over the wetted surface, the second-order wave excitation force has been calculated. The maximum force applied on the floating cylinder becomes non-dimensional when considering it with and without the fixed cylinder. The results showed the effect that the existence of the fixed cylinder had on the increase in the second-order forces is quite evident where, for a significant parameter of the floating cylinder, the force in the heave direction was enhanced by up to 1.55 times.

Introduction

The forces from second-order and low-frequency waves exert an important influence on the dynamics of floating objects. These forces are recognized as wave drift forces, which result in a slow and steady drift motion in the direction of the wave. Although the forces from the first-order wave involve a significant portion of body excitation, second-order theories are important in some surrounding circumstances in order to calculate the nonlinear effects of the wave. In these theories, the condition of flow impermeability into the object on the wetted surface is considered to be more precise. In the solving procedure of second-order equations, all of the terms related to velocity potential function, fluid pressure and wave forces, which have a linear relationship with wave amplitude and the second power of the wave amplitude, are considered. Furthermore, the nonlinear velocity effects of fluid particles on the free surface are also considered. Second-order equations include moderate forces and oscillating forces with frequencies greater or less than the frequency of the wave.

Direct or indirect methods for solving equations including second-order potentials have been adopted in various studies (Chau & Eatock Taylor, 1992; Huang & Eatock Taylor, 1996; Teng & Kato, 1999). Vazquez (Vazquez, 1997) combined BEM and the indirect method to develop a method for calculating second-order hydrodynamic loads on marine structures caused by multi-directional waves. Renaud et al. (Renaud et al., 2008) developed mid-field formulas for multi-directional collisions of waves and carried out calculations for the progressive wave forces and low-frequency forces of a liquefied

natural gas (LNG) carrier ship. Lupton and Langley (Lupton & Langley, 2017) investigated the scaling of small drift motions with regard to platform size including mooring characteristics and wave conditions. They also developed a frequency-domain model of a flexible floating wind turbine structure with first and second-order hydrodynamic loading. Lim and Kim (Lim & Kim, 2018) designed a new wave method to estimate the extreme slow-drift motion of moored offshore platforms. The accuracy and applicability of this new method were tested through a series of simulations using a semi-submersible model. Pegalajar-Jurado and Bredmose (Pegalajar-Jurado & Bredmose, 2019) investigated a numerical model that includes both inviscid slow-drift forcing through full quadratic transfer functions (QTFs) and viscous forcing. The damping ratios estimated by Operational Modal Analysis were found to be similar to the calibrated values for mild pink-noise sea states, while significant differences exist for the stronger Pierson-Moskowitz sea states. Abyn et al. (Abyn et al., 2016) investigated the hydrodynamic interaction between a tension leg platform (TLP) and a semi-submersible (Tender Assisted Drilling) for regular waves. A floating production storage and offloading unit (FPSO) and a semisubmersible platform's interactions in regular waves were investigated by Ghafari et al. (Ghafari et al., 2019) using the BEM in the ANSYS/AQWA software. The mean and slowly varying wave drift forces on a moored semi-submersible platform were investigated by Hu and Zhou (Hu & Zhou, 2017). The hydrodynamic interaction between several floating cylinders was investigated by Ali and Khalil (Ali & Khalil, 2005) through the application of a 3D source-sink method. Based on a viscous computational fluid dynamics (CFD) model, a framework analysis was developed to determine the behavior of a partially-entrapped volume of water between two floating bodies (Chua, Eatock Taylor & Choo, 2018). Jin et al. (Jin et al., 2018) investigated the interactions between two ships in regular waves by using the viscous unsteady Reynolds-Averaged Navier-Stokes (URANS) method. The focus of the presented study was the changes in the second-order forces related to the different parametric aspects of two cylinders when considering the effect of wave diffraction and comparing the results with the single cylinder case. Zhang et al. (Zhang et al., 2013) studied the low-frequency horizontal motions of a multi-point moored FPSO unit and the second-order wave drift forces.

In the open ocean, low-frequency second-order forces result in the excitation and subsequent drift of objects, such as ships, wave energy converter devices, mooring lines, oil slicks and even ice flows. To make the importance of second-order forces clear using an example; in offshore wave energy converter farms, the existence of several elements side by side will cause a depression in wave energy and, eventually, high-frequencies wave energies; these are gradually converted to low-frequency

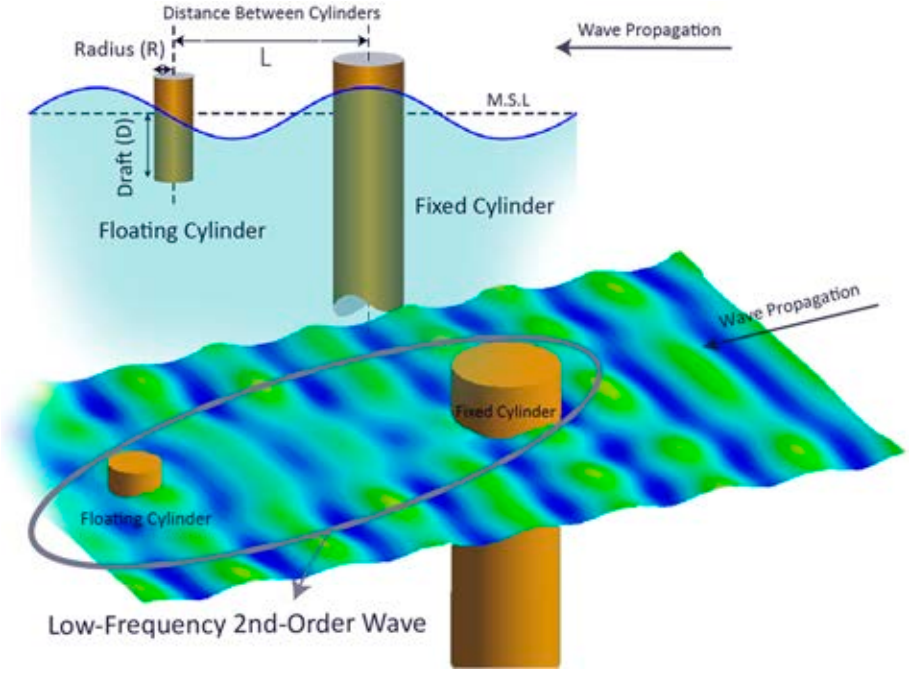

Figure 1. Floating and fixed tandem cylinders under the effect of an incident wave

wave energies: so-called second-order hydrodynamic forces. In fact, the converters will become second-order wave energy converters. In all the research into second-order hydrodynamic forces, the interaction of the wave and a structure, when considering low-frequency second-order wave forces, especially for parametric multi-structure interaction, has rarely been studied. This paper has presented the effect of the variation in the parameters of a floating cylinder (such as draft) and the interaction of the distance between two fixed and floating cylinders. Low-frequency second-order hydrodynamic wave forces were applied to a floating cylinder, caused by wave diffraction. Figure 1 has shown the floating and fixed cylinders under the effect of an incident wave. The distance between the two cylinders (L), the draft (D) and the radius (R) have been shown in this figure.

Governing equations

Potential theory

Considering the Laplace equation as the governing equation, the velocity potential of the fluid flow field that surrounds a floating object, can be defined as follows (Barltrop, 1998):

$$\Phi\left(\vec{X},t\right)= a_w\varphi\left(\vec{X}\right)\mathrm{e}^{-i\omega t} \tag{1}$$

where, a_w and ω are the incident wave's amplitude and the wave's frequency respectively, and the expression $\varphi\left(\vec{X}\right)$ is composed of three components that include the first-order incident wave potential (φ_I) with unit wave amplitude, the corresponding diffracted wave potential (φ_d) and the radiation wave potential (φ_{rj}) due to the j-th motion with unit motion amplitude. Therefore, the velocity potential equation can be written as follows (Barltrop, 1998):

$$\varphi\left(\vec{X}\right)\mathrm{e}^{-i\omega t}=\left[\left(\varphi_I+\varphi_d\right)+\sum_{j=1}^{6}\varphi_{rj}x_j\right]\mathrm{e}^{-i\omega t} \tag{2}$$

By considering an incompressible, non-viscous and irrational flow, the velocity potential function can be obtained from the solution to the Laplace equation in the entire fluid domain as follows:

$$\Delta\varphi=\frac{\partial^2\varphi}{\partial X^2}+\frac{\partial^2\varphi}{\partial Y^2}+\frac{\partial^2\varphi}{\partial Z^2}=0 \tag{3}$$

The behavior of the fluid-structure interaction is described by the following set of boundary conditions:

$$\begin{aligned}
&-\omega^2\varphi+g\frac{\partial\varphi}{\partial Z}=0 \ \text{ for } \ Z=0\\
&\frac{\partial\varphi}{\partial n}=\begin{cases}-i\omega n_j & \text{for radiation potential}\\ -\frac{\partial\varphi}{\partial n} & \text{for diffraction potential}\end{cases}\\
&\frac{\partial\varphi}{\partial Z}=0 \ \text{ for } \ Z=-d\\
&\left|\nabla\varphi\right|\to 0 \ \text{ when } \ \sqrt{x^2+y^2}\to\infty
\end{aligned} \tag{4}$$

The boundary integration method is used to solve the fluid velocity potential function which is satisfied by the boundary conditions. In this method, the frequency domain pulsating Green's function in water of finite depth is introduced; this obeys the boundary conditions defined in Eq. (4). More details of the methodology and computational implementation can be found in the literature (Ghafari & Dardel, 2018).

Second-order wave force

The second-order wave excitation force concept can be explained by considering the hydrodynamic responses supposition of a fixed or floating body surrounded by an incompressible, irrotational, homogeneous and inviscid fluid. Furthermore, in this hypothesis, both the body's motion response amplitude and the wave's amplitude are assumed to be small. With these assumptions, the velocity potential function can be used to characterize the surrounding fluid. The second-order wave excitation force and moment can be calculated in the following manner (Pinkster, 1980):

$$\begin{aligned}
\vec{F}^{(2)}=&-\frac{1}{2}\rho g\oint_{WL}\zeta_r^{(1)}\cdot\zeta_r^{(1)}\vec{n}dl && \text{Water line integral}\\
&+\frac{1}{2}\rho\iint_{S_0}\left[\nabla\Phi^{(1)}\cdot\nabla\Phi^{(1)}\right]\vec{n}dS && \text{Bernoulli}\\
&+\rho\iint_{S_0}\left[\vec{X}^{(1)}\cdot\nabla\frac{\partial\Phi^{(1)}}{\partial t}\right]\vec{n}dS && \text{Acceleration}\\
&+\vec{\alpha}^{(1)}\times\vec{F}^{(1)} && \text{Momentum}\\
&+\rho\iint_{S_0}\frac{\partial\Phi^{(2)}}{\partial t}\vec{n}dS && \text{Second-order potential}
\end{aligned} \tag{5}$$

$$\vec{M}^{(2)} = -\frac{1}{2}\rho g \oint_{WL} \zeta_r^{(1)} \cdot \zeta_r^{(1)} (\vec{x} \times \vec{n})\, dl \quad \text{Water line integral}$$

$$+\frac{1}{2}\rho \iint_{S_0} \left[\nabla\Phi^{(1)} \cdot \nabla\Phi^{(1)}\right](\vec{x} \times \vec{n})\, dS \quad \text{Bernoulli}$$

$$+\rho \iint_{S_0} \left[\vec{X}^{(1)} \cdot \nabla \frac{\partial \Phi^{(1)}}{\partial t}\right](\vec{x} \times \vec{n})\, dS \quad \text{Acceleration}$$

$$+\vec{\alpha}^{(1)} \times \vec{M}^{(1)} \quad \text{Momentum}$$

$$+\rho \iint_{S_0} \frac{\partial \Phi^{(2)}}{\partial t}(\vec{x} \times \vec{n})\, dS \quad \text{Second-order potential} \qquad (6)$$

where, S_0 is the mean wetted surface, $\zeta_r^{(1)} = \zeta^{(1)} - X_{3WL}^{(1)}$ is the relative wave elevation along the mean undisturbed water line and $\vec{F}^{(1)}$ and $\vec{M}^{(1)}$ are the total first order fluid force and the moment, respectively.

Equations of motion

Through the interaction of the body (Figure 2) with the frequency dependent hydrodynamic coefficients, a set of linear motion equations can be derived as follows:

$$\left[-\omega_e^2(M_s + M_a) - i\omega_e C + K_{hys}\right]\left[x_j\right] = \left[F_j\right] \qquad (7)$$

In Eq. (7), M_s is a 6×6 structural mass matrix, $M_a = [A_{jk}]$ and $C = [B_{jk}]$, are the hydrodynamic added mass and damping matrices which include the interaction coupling terms between two structures, the stiffness matrix (K_{hys}) is a combined hydrostatic stiffness matrix and F_j denotes the total forces and moments.

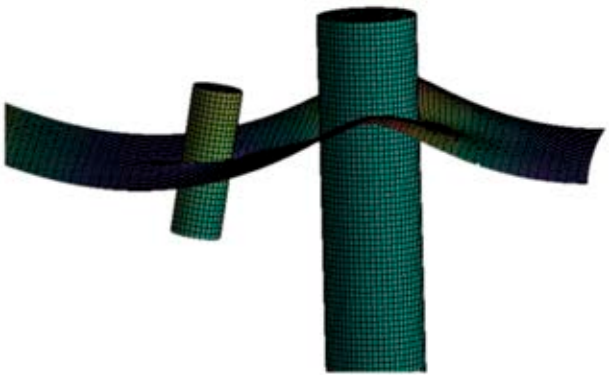

Figure 2. Motion of the floating cylinder

Validation

For verification purposes, the experimental test results of a restrained cylinder body were used to represent a vertical cylinder (Fonseca, 2011). The experimental work for the restrained body was carried out at an offshore shallow water wave basin belonging to the Danish Hydraulic Institute (DHI). This basin is 3 m deep, 30 m long and 20 m wide and has a hydraulic flap wave maker. The applied mean drift forces in the heave and surge directions were measured using the radiation of a monochromatic wave. Table 1 presents the characteristics of the waves that were tested (Fonseca et al., 2011).

Figure 3 has shown a comparison of the non-dimensional drift force coefficients (F_{2nd}) and the heave and the surge drift forces versus the wave period. The forces were non-dimensionalized as: $F_{2nd}/(\rho g A^2 l)$, where g, ρ and A are acceleration due to gravity, fluid density and wave amplitude, respectively. l was defined as the characteristic length and was considered to be equal to 1 m. A comparison of the results of the numerical and experimental drift

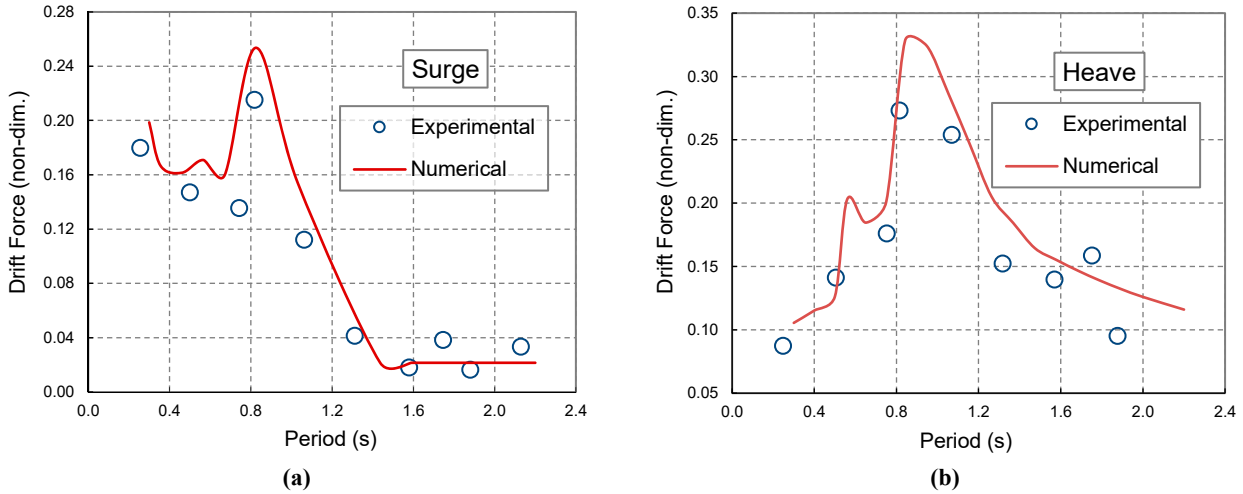

Figure 3. Comparison of the non-dimensional drift force for the surge (a) and heave (b) motions of the wave

Table 1. Characteristics of the tested monochromatic wave

Wave index	Period (s)	Amplitude (cm)
1	0.70	1.1
2	0.90	1.6
3	1.10	2.2
4	1.15	2.3
5	1.35	2.9
6	1.75	4.0
7	1.90	4.4
8	2.00	4.7
9	2.20	4.8
10	1.55	3.4

of a restrained cylinder body in both the surge and heave directions has been shown in Figure 3. As can be seen in the figures, there is relatively good agreement between the numerical results and the experimental data.

Results and discussion

In this section, the effect of the distance between two fixed and floating cylinders on the drift force acting on the floating cylinder has been investigated. The incident wave is diffracted by the fixed cylinder, and as a result, low-frequency waves are radiated by the floating cylinder. The wave patterns for different wave frequencies have been shown in Figure 4. Under this excitation, the unrestrained floating cylinder will drift away and move in a slow steady drift motion along the direction of the incident wave. The drift forces were calculated using the varying three parameters of distance and draft (L and D). The non-dimensional parameters of L/R, D/R and $(F - F_0)/F_0$ were defined, where F and F_0 denote the maximum force applied to the floating cylinder with and without considering the existence of the fixed cylinder, respectively. In all of the analyses, the fixed and floating cylinders had radiuses of 2 m and 1 m, respectively. The flow cylinder draft varied between 2, 3 and 4 m and the distance between the two cylinders was changed from 4 m up to 40 m with an interval of 1 m. Therefore, D/R had three cases (D/R = 2, 3 and 4) and L/R had 37 cases (L/R = 4 up to 40). Hence, the total calculation cases were 37×3, which is equal to 111 cases. In this analyzed case, the incident wave frequency was set as 2.51 rad/s with a phase angle of 0–2π.

The numerical results from $(F - F_0)/F_0$ versus L/R for different values of D/R (= 2, 3 and 4) have been shown in Figure 5. As the value of L/R

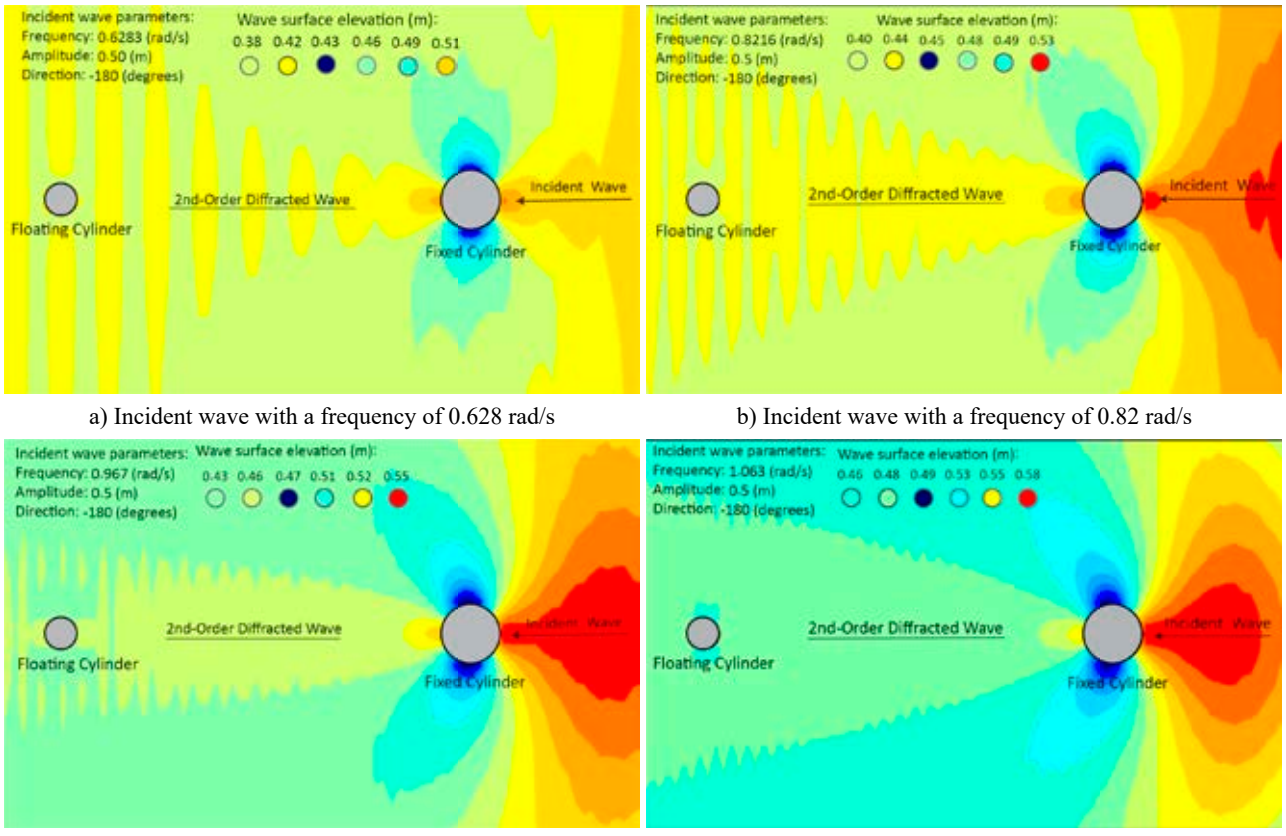

a) Incident wave with a frequency of 0.628 rad/s

b) Incident wave with a frequency of 0.82 rad/s

c) Incident wave with a frequency of 0.967 rad/s

d) Incident wave with a frequency of 1.063 rad/s

Figure 4. Wave patterns for different wave frequencies

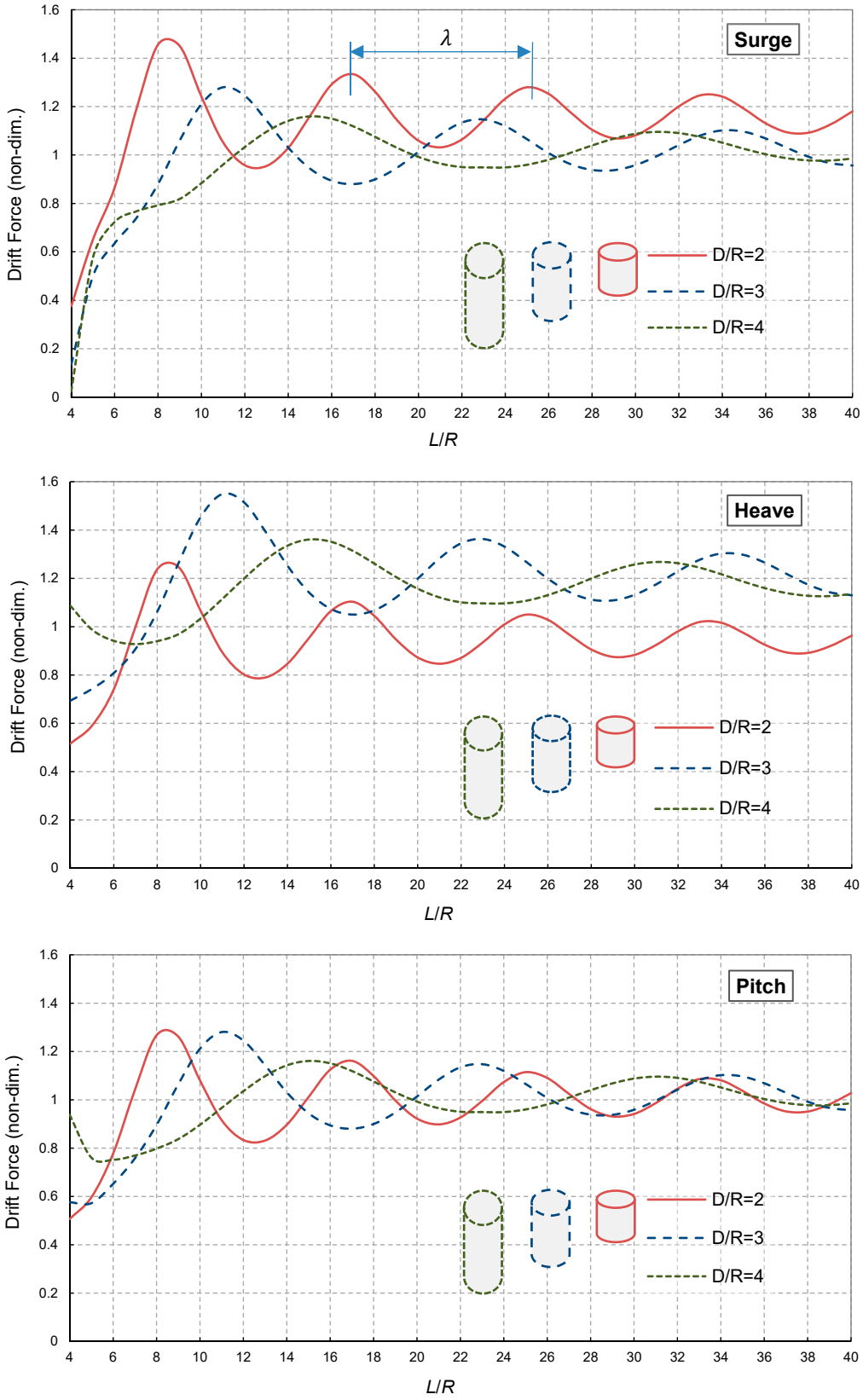

Figure 5. Numerical results of $(F - F_0)/F_0$ versus L/R under different values of D/R

increased, all of the drift forces (surge, heave, and pitch) had a regular sinusoidal and transient trend and the rate of damping in the intensity of the interaction decreased because of the three-dimensional wave propagation and hence the decrease in the wave-energy density per unit area on the free surface and eventually, the amplitude of the force operator was diminished. The effect of the fixed cylinder in

Table 2. Comparison of the maximum values of $(F - F_0)/F_0$ for different values of D/R

The n-th Crest	The Three Motions								
	Surge			Heave			Pitch		
	$D/R = 2$	$D/R = 3$	$D/R = 4$	$D/R = 2$	$D/R = 3$	$D/R = 4$	$D/R = 2$	$D/R = 3$	$D/R = 4$
1st	1.46	1.28	1.16	1.25	1.55	1.36	1.27	1.28	1.16
2nd	1.33	1.15	1.10	1.10	1.36	1.27	1.16	1.15	1.10
3th	1.28	1.10	–	1.05	1.30	–	1.11	1.10	–
4th	1.25	–	–	1.02	–	–	1.09	–	–
Distance between peaks (λ)	8 m	12 m	16 m	8 m	12 m	16 m	8 m	12 m	16 m

increasing the second-order forces is quite evident in which, at $D/R = 3$, the force in the heave direction was enhanced by up to 1.55 times. By enhancing D/R, in each of the surge, heave and pitch motions, the number of force response cycles decreased and the distance between two adjacent crests (λ) of the drift force trend also increased.

The maximum values of $(F - F_0)/F_0$ and the distance between the adjacent peaks (λ) for different values of D/R for the three motions of surge, heave and pitch have been compared in Table 2. As can be seen in Table 2, the maximum reduction between the first and last peak of $(F - F_0)/F_0$ in surge, heave and pitch for $D/R = 2$ was 14.38%, 18.40% and 14.17%, respectively, while these values decreased by 14.06%, 16.12% and 14.06% for $D/R = 3$. For $D/R = 4$ the amount of decline was less, about 5.2%, 6.6% and 5.2% for surge, heave and pitch, respectively. Hence, it can be concluded that the greatest reduction occurred for $D/R = 2$ for the heave motion, while the smallest changes occurred in the surge and pitch motion directions when $D/R = 4$.

In order to compare the drift force and L/R, the maximum values of the drift force which were acting on the floating cylinder at D/R=2 and for different values of L/R, have been shown in Figure 6. As can be seen, by placing the floating cylinder at a distance of 4 m from the fixed cylinder, the floating cylinder was located in the lee area of the rigid fixed cylinder. Therefore, the cylinder was positioned in a safe area with the least amount of applied force. As the distance of the floating cylinder to the fixed cylinder increased, the floating cylinder was gradually exposed to waves with greater amplitude; hence it was subjected to the most energy at a distance of 9 m. Beyond the 9 m distance, the floating cylinder was exposed to both induced first-order and low-frequency drift wave forces. As the distance between the two cylinders increased, the wave diffraction was slightly decreased. As shown in Figure 6, as L/R increased, the drift force ratio for the surge motion showed more fluctuation than the pitch and heave motions. It should be noted that the maximum and minimum force ratios occurred with the placement of the floating cylinder on the peak and trough of the incident wavelength, respectively. For all of the three motions, the maximum and minimum force ratios occurred at identical values of L/R.

Conclusions

In this paper, the drift forces exerted in the case of two fixed and floating cylinders and the interactions for three different drafts and distances between

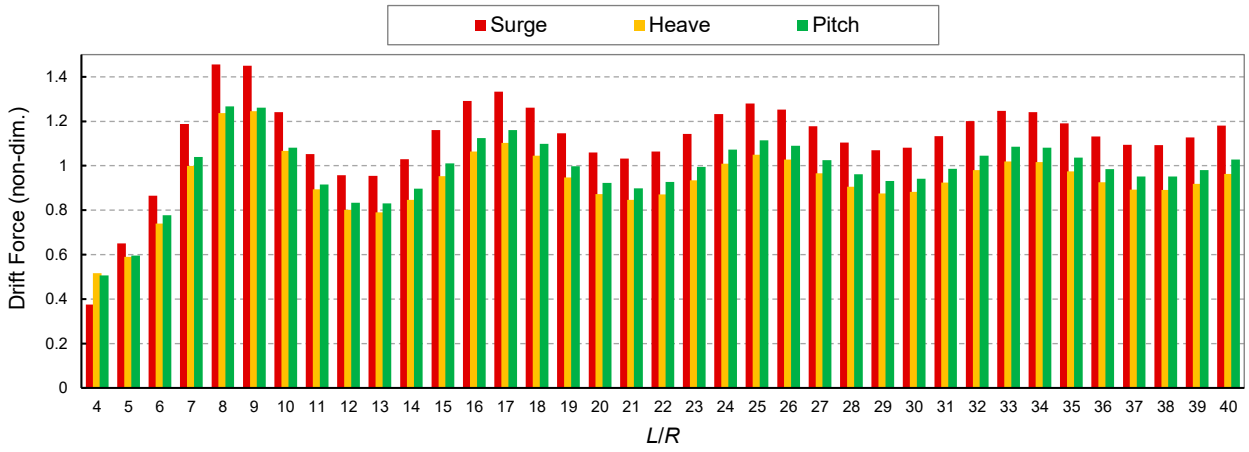

Figure 6. $(F - F_0)/F_0$ versus L/R for $D/R = 2$ for the surge, heave and pitch motions

them has been investigated. The main results of these analyses are as follows:

- When the distance between the two cylinders was increased, the drift forces displayed a sinusoidal damped and transient property.
- With increasing values of L/R, the drift force ratio for the surge motion showed more fluctuations than the pitch and heave motions.
- As the value of D/R was enhanced, the response fluctuations of the drift forces were reduced.
- By increasing the value of D/R, the maximum values of $(F - F_0)/F_0$ occurred for higher values of L/R.
- With increasing values of D/R, the maximum amount of drift force decreased in the surge direction.
- Depending on the position of the floating cylinder, the presence of the fixed cylinder can have a positive or negative effect on the enhancement of the drift force.

References

1. Abyn, H., Islam, M.R., Maimun, A., Mahmoudi, A. & Kato, J. (2016) Experimental Study of Motions of Two Floating Offshore Structures in Waves. *Brodogradnja* 67(2), pp. 1–13.
2. Ali, M.T. & Khalil, G.M. (2005) *On hydrodynamic interaction between several freely floating vertical cylinders in waves*. ASME 2005 24th International Conference on Offshore Mechanics and Arctic Engineering. June 12–17, 2005, Halkidiki, Greece. American Society of Mechanical Engineers Digital Collection, pp. 391–398.
3. Barltrop, N.D.P. (1998) *Floating Structures: A guide for design and analysis*. CMPT.
4. Chau, F.P. & Eatock Taylor, R. (1992) Second-order wave diffraction by a vertical cylinder. *Journal of Fluid Mechanics* 240, pp. 571–599.
5. Chua, K.H., Eatock Taylor, R. & Choo, Y.S. (2018) Hydrodynamic interaction of side-by-side floating bodies part I: Development of CFD-based numerical analysis framework and modified potential flow model. *Ocean Engineering* 166, pp. 404–415.
6. Fonseca, N., Pessoa, J., Mavrakos, S. & Le Boulluec, M. (2011) Experimental and numerical investigation of the slowly varying wave exciting drift forces on a restrained body in bi-chromatic waves. *Ocean Engineering* 38 (17–18), pp. 2000–2014.
7. Ghafari, H. & Dardel, M. (2018) Parametric study of catenary mooring system on the dynamic response of the semi-submersible platform. *Ocean Engineering* 153, pp. 319–332.
8. Ghafari, H.R., Ketabdari, M.J., Ghassemi, H. & Homayoun, E. (2019) Numerical study on the hydrodynamic interaction between two floating platforms in Caspian Sea environmental conditions. *Ocean Engineering* 188, 106273.
9. Hu, J. & Zhou, L. (2017) Experimental and numerical study on wave drift forces on a semi-submersible platform in waves. *Ships and Offshore Structures* 12(1), pp. 56–65.
10. Huang, J.B. & Eatock Taylor, R. (1996) Semi-analytical solution for second-order wave diffraction by a truncated circular cylinder in monochromatic waves. *Journal of Fluid Mechanics* 319, pp. 171–196.
11. Jin, Y., Chai, S., Duffy, J., Chin, C. & Bose, N. (2018) URANS predictions on the hydrodynamic interaction of a conceptual FLNG-LNG offloading system in regular waves. *Ocean Engineering* 153, pp. 363–386.
12. Lim, D.-H. & Kim, Y. (2018) Design wave method for the extreme horizontal slow-drift motion of moored floating platforms. *Applied Ocean Research* 71, pp. 48–58.
13. Lupton, R.C. & Langley, R.S. (2017) Scaling of slow-drift motion with platform size and its importance for floating wind turbines. *Renewable Energy* 101, pp. 1013–1020.
14. Pegalajar-Jurado, A. & Bredmose, H. (2019) Reproduction of slow-drift motions of a floating wind turbine using second-order hydrodynamics and Operational Modal Analysis. *Marine Structures* 66, pp. 178–196.
15. Pinkster, J.A. (1980) *Low frequency second order wave exciting forces on floating structures*. Doctoral thesis. TU Delft.
16. Renaud, M., Rezende, F., Waals, O., Chen, X.-B. & van Dijk, R. (2008) *Second-order wave loads on a LNG carrier in multi-directional waves*. ASME 2008 27th International Conference on Offshore Mechanics and Arctic Engineering. June 15–20, 2008, Estoril, Portugal. American Society of Mechanical Engineers Digital Collection, pp. 363–370.
17. Teng, B. & Kato, S. (1999) A method for second-order diffraction potential from an axisymmetric body. *Ocean Engineering* 26(12), pp. 1359–1387.
18. Vazquez, J.H. (1995) *Hydrodynamic loads on offshore structures in bichromatic bidirectional seas*. Doctoral thesis. University of Houston.
19. Zhang, L.R., Lu, H., Yang, J., Peng, T. & Xiao, L. (2013) Low-frequency drift forces and horizontal motions of a moored FPSO in bi-directional swell and wind-sea offshore West Africa. *Ships and Offshore Structures* 8(5), pp. 425–440.